7-2013

Ground Shock Resistance of Mechanically Stabilized Earth Walls

Christopher Y. Tuan
University of Nebraska-Lincoln, ctuan@unomaha.edu

International Journal of Geomechanics. Submitted January 29, 2013; accepted July 24, 2013;
posted ahead of print July 26, 2013. doi:10.1061/(ASCE)GM.1943-5622.0000342

Ground Shock Resistance of Mechanically Stabilized Earth Walls

Christopher Y. Tuan[1], Ph.D., P.E., F.ASCE

ABSTRACT

A simple analytical method has been developed that characterizes plane shock wave propagation through reinforced soil and the dynamic interaction between soil and retaining wall panels. The shock wave due to an explosion in the backfill was modeled as a velocity boundary condition at a standoff distance from the wall. The exact solution to this problem was obtained using the Laplace transform method. Full-scale explosive test data from 4.6-m high and 24-m wide reinforced soil walls were used to validate the analytical methodology. The accuracy of the analytical method has further been verified by finite element analysis. The method is adequate for the response analysis of mechanically stabilized embankment walls under ground shock due to an explosion in the backfill.

KEY WORDS: Reinforced soil, Mechanically stabilized embankment, Finite element analysis, Ground shock, Stability analysis, Analytical modeling.

[1]Professor, Department of Civil Engineering, University of Nebraska-Lincoln, Peter Kiewit Institute, 1110 S. 67th Street, Omaha, Nebraska 68182-0178, U.S.A. E-mail: ctuan1@unl.edu.

International Journal of Geomechanics. Submitted January 29, 2013; accepted July 24, 2013;
posted ahead of print July 26, 2013. doi:10.1061/(ASCE)GM.1943-5622.0000342

INTRODUCTION

Mechanically stabilized embankment (MSE) is constructed with reinforcing strips or meshes embedded between lifts of soil layers, which has been used for retaining walls, bridge abutments, dams, seawalls, and levees. Although the basic concepts were centuries old, MSE in its current form was developed in the 1960's. Commonly used reinforcing elements include steel strips and geosynthetics (i.e., geogrids and geomembranes), though micropiles have also been used to reinforce or stabilize earth embankmants (e.g., Esmaeili et al. 2012). The design of MSE walls, also known as reinforced soil walls, consists of determining the geometric and reinforcement requirements to prevent various internal and external failures caused by gravity, seismicity and other loading effects. The most common failure of MSE walls is due to pullout of soil reinforcement. Bathurst et al. (2012) used 318 geogrid pullout tests to calibrate the load and resistance factors for use in the limit state design of reinforced soil walls. Zhou et al. (2012) studied the interaction between sand particles and the transverse ribs of geogrids in pullout tests, which revealed a punching shear failure mechanism. Giang et al. (2010) conducted pullout tests with different types of geogrids to evaluate the influence of transverse ribs and the dilatancy characteristics of sand during unload-reload processes. Berg et al. (2009) developed guidelines for the design and construction of MSE walls and reinforced soil slopes.

The objective of this study is to develop a simple analytical method for design of MSE walls to resist ground shock loading due to an explosion in the backfill. Richardson et al. (1977) conducted explosive tests in the backfill of a 6-m (20-ft) high MSE wall for a seismic response study, which revealed good ground shock resistance. The field explosive tests conducted by Raudanski et al. (1990) and Reid (1995) have shown that such structures are survivable under strong ground shock and may be used for protective shelters such as shown in Figure 1. Precast

International Journal of Geomechanics. Submitted January 29, 2013; accepted July 24, 2013;
posted ahead of print July 26, 2013. doi:10.1061/(ASCE)GM.1943-5622.0000342

concrete panels attached to horizontal metal strips in a backfill were utilized in that construction. A typical wall can be constructed with interlocking modular panels. Soil reinforcement in the form of meshes or grids, are connected to the back of the modular panels and embedded in different lifts of soil layers. Ground shock wave propagation through reinforced soil and the dynamic interaction with retaining wall panels have been studied analytically. The governing differential equation and the associated boundary conditions are presented, and closed-form solutions are obtained and compared to the data from full-scale explosive tests by Reid (1995). The accuracy of the analytical model is further verified by a transient dynamic finite element analysis.

SOIL UNDER BLAST LOADING

Many civil and military projects such as mining, tunnels, and underground shelters, involve high strain rate soil dynamics. Soil behavior under blast loading has been studied by many researchers (Wang and Lu 2003; Grujicic et al. 2008; An et al. 2011). Soil is an assemblage of individual particles rather than a continuum and may have various degrees of water saturation. The rapid release of energy from a buried explosion causes a sudden rise of pressure or a shock front propagating through the soil medium. These conditions have posed challenges to accurately predicting soil behavior under blast loading. Therefore, common practice in modeling soil behavior under blast loading is mainly based on empirical formulae from field tests (Drake and Little 1983). Since conditions varied in different test sites, predictions on the ground shock intensity using those empirical formulae scatter significantly. Differences in soil stress and ground motion at the same scaled distance could be more than two orders of magnitude between dry and saturated soils. Soils cannot sustain tension and any tension developed in the soil will be

International Journal of Geomechanics. Submitted January 29, 2013; accepted July 24, 2013;
posted ahead of print July 26, 2013. doi:10.1061/(ASCE)GM.1943-5622.0000342

taken by the soil reinforcement fully anchored in the soil. For water-bearing soil under gradual static loading, the water and air will be pressed out of the voids and the compressibility mainly depends upon the solid skeleton. Under blast loading, on the other hand, the duration is not long enough for the air and water to flow through the soil skeleton. Rather, water and air voids will deform with the skeleton. Therefore, the rate dependency must be considered for soil responses under blast loading. Since the air and water are trapped within soil voids and deform with the soil skeleton under blast loading, relative movement between the skeleton and the water and air can be neglected. Therefore, even though soil is a three-phase material at the micro level, it may be considered as a single-phase material at the macro level.

DESIGN PARAMETERS OF AN MSE WALL

As specified in Chapter 4 of the FHWA design guidelines (Berg et al. 2009), the primary parameters of an MSE wall design are the wall embedment, the vertical spacing of the soil reinforcement layers, and the reinforcement length. The embedment depth at the front of the wall is measured from ground level to the top of footing or leveling pad, with a minimum of 0.61 m (2 ft). Depending upon frost penetration, shrinkage and swelling of foundation soil, seismicity and scour, larger values may be required. The vertical spacing of the reinforcement is usually controlled by the type of facing panels and facing connection locations. The maximum spacing should be limited to twice the thickness of the modular concrete facing unit or 80 cm (2.7 ft), whichever is less. It should be a multiple of the compacted lift thickness required for fill placement. Typical compacted lift thickness is in the range of 20 to 30 cm (8 to 12 in.). Traditionally the minimum reinforcement length for MSE wall construction should be the greater of 0.7 H or 2.5 m (8 ft), where H is the wall height.

International Journal of Geomechanics. Submitted January 29, 2013; accepted July 24, 2013;
posted ahead of print July 26, 2013. doi:10.1061/(ASCE)GM.1943-5622.0000342

ANALYSIS OF AN MSE WALL UNDER GROUND SHOCK

For an MSE wall subjected to ground shock from backfill, the maximum tensile forces in different reinforcement layers occur at the connection with facing panels. However, these forces occur at different time instants depending upon the arrival times of a shock wave at different facing panels. Figure 2 shows the free-body diagram of a single facing panel connected to two layers of geogrids. The interface soil pressure, $\sigma_i(t)$, acting on the facing panel is resisted by tensile forces developed in the soil reinforcement when relative displacement between soil and reinforcement takes place. The shear and frictional forces, F_v, developed between interlocking panels are ignored. The facing panel connection with the reinforcement should be designed to fully develop the pull-out resistance without rupture or excessive deformation. Further, the reinforcement should have adequate ductility and tensile strength to accommodate significant panel displacement.

Ground Shock due to Explosion in the Backfill

Crawford, Higgins and Bultmann (1974) stated that the normal stress acting across the interface between soil and a buried structure due to ground shock can be expressed as

$$\sigma_i(t) = \sigma_{ff} \pm \rho c \, \Delta V(t) \tag{1}$$

where σ_{ff} is the free-field incident stress produced by the explosion, $\Delta V(t)$ is the velocity differential between the free-field particle velocity at the location of structure surface and the velocity of the structure at the same point, and ρc is the soil acoustic impedance. The sign of the second term in Eq.(1) is taken positive for incident faces and negative for reactive faces. Drake

International Journal of Geomechanics. Submitted January 29, 2013; accepted July 24, 2013;
posted ahead of print July 26, 2013. doi:10.1061/(ASCE)GM.1943-5622.0000342

and Rochefort (1987) showed that Eq.(1) is actually a statement of continuity for both stress and displacement at the interface between the soil and structure, and the interface stress is

$$\sigma_i = \sigma_{ff} + \rho c_L \left(V_{ff} - \dot{u} \right) \quad = \quad 2\sigma_{ff} - \rho c_L \dot{u} \tag{2}$$

where ρ is the mass density and c_L the loading wave velocity of the soil, and V_{ff} is the free-field particle velocity associated with σ_{ff}, and $\dot{u}$ is the velocity of the structure.

A closed-form solution has been obtained by Tuan and Merkle (1993) to determine the rigid body lateral movement of an MSE wall under ground shock loading. This single-degree-of-freedom (SDOF) model is shown in Figure 3. The layers of soil reinforcement are assumed to run parallel to the ground shock wave direction and the soil and wall panel to stay bonded at the interface. The particle displacement in a homogeneous medium, $u(x,t)$, in a wave equation can be expressed as

$$\frac{\partial^2 u}{\partial t^2} \quad = \quad c^2 \frac{\partial^2 u}{\partial x^2} \tag{3}$$

where c is the wave propagation velocity of the reinforced soil, and approximated by

$$c \quad \approx \quad \sqrt{\frac{K_x}{\rho}} \tag{4}$$

where K_x and ρ are the bulk modulus and the mass density of the reinforced soil, respectively. For ground shock loading, the loading wave velocity c_L is used along with the unloading bulk modulus in Eq.(4).

At $x = 0$, the shock wave front, having an initial free-field particle velocity, v_o, arrives at time $t = 0$ and decays exponentially, so that

International Journal of Geomechanics. Submitted January 29, 2013; accepted July 24, 2013;
posted ahead of print July 26, 2013. doi:10.1061/(ASCE)GM.1943-5622.0000342

$$\frac{\partial u}{\partial t}(0,t) = v_o\, e^{-\alpha t} \qquad (t > 0) \tag{5}$$

where α is the particle velocity attenuation rate. At $x = R$, the equation of motion of the wall panel is

$$M\frac{\partial^2 u}{\partial t^2} = -\sigma_i\, h\, b - K(u)\,u \tag{6}$$

where M is the mass and $K(u)$ is the structural stiffness of the wall panel, which is generally a function of the wall panel displacement. Expressing the interface soil stress, $\sigma_i(t)$, in terms of the wall panel displacement, Eq.(6) becomes

$$\mu\frac{\partial^2 u}{\partial t^2} + \frac{\partial u}{\partial x} + \frac{K(u)\,u}{K_x\, h b} = 0 \tag{7}$$

where

$$\mu = \frac{M}{K_x\, h b} \tag{8}$$

The unit resistance function, defined as the structural resistance per unit area of wall panel, can be expressed as

$$R(u) = \frac{K(u)u}{hb} \tag{9}$$

The unit resistance function $R(u)$ may be modeled as linearly elastic, elastoplastic, perfectly plastic, or other appropriate models. However, the high strain rate under a strong incident shock would produce perfectly plastic response, if the MSE wall were designed to be ductile. Assuming the wall response is perfectly plastic, then $R(u) = R_{\max}\, F(t-T)$, where $F(t-T)$ is the Heaviside step function defined as: $F(t-T) = 0$ if $t < T$ and $F(t-T) = 1$ if $t \geq T$, T is the arrival

International Journal of Geomechanics. Submitted January 29, 2013; accepted July 24, 2013;
posted ahead of print July 26, 2013. doi:10.1061/(ASCE)GM.1943-5622.0000342

time of the shock wave, and the ratio of unit resistance to the constrained reinforced soil modulus becomes a constant

$$\lambda = \frac{R_{\max}}{K_x} \tag{10}$$

The wall panel and reinforced soil system was at rest before ground shock arrives, therefore,

$$u(x,0) = 0 \qquad (0 \le x \le R) \tag{11}$$

$$\frac{\partial u}{\partial t}(x,0) = 0 \qquad (0 \le x \le R) \tag{12}$$

The closed form solution to the governing equation and the associated boundary and initial conditions was obtained by using the Laplace transform method as given in the Appendix. The closed-form solution gives the same interface stress as given by Eq.(2), provided the wall panel stays in contact with the soil. Even though the closed-form solution accounts for superposition of incident and reflected waves propagating between the explosion source and the interface, it gains little advantage over Drake's model, since in reality stress waves decay rapidly with distance.

Based on Eqs.(2) and (6), the equation of motion of the wall panel can be shown to be

$$\rho_w d \frac{\partial^2 u}{\partial t^2} + \rho c_L \frac{\partial u}{\partial t} + R(u) = 2\sigma_{ff} \tag{13}$$

where ρ_w is the mass density and d is the thickness of the wall panel, c_L is the loading wave velocity of the reinforced soil, and $R(u)$ is the total pull-out resistance of geogrids per unit area of the wall panel. The free-field soil normal stress, σ_{ff}, due to a buried explosion at a certain standoff, can be approximated by an exponentially decaying wave,

$$\sigma_{ff} = \sigma_o e^{-\alpha(t-T)} \qquad (t > T) \tag{14}$$

International Journal of Geomechanics. Submitted January 29, 2013; accepted July 24, 2013;
posted ahead of print July 26, 2013. doi:10.1061/(ASCE)GM.1943-5622.0000342

where σ_o is the peak free-field stress and α is the normal stress decay rate, and σ_o is related to the initial free-field particle velocity as

$$\sigma_o = \rho c_L v_o \tag{15}$$

The corresponding free-field soil displacement time-history is

$$u_{ff} = \frac{\sigma_o}{\alpha \rho c_L}\left[1 - e^{-\alpha(t-T)}\right] \qquad (t > T) \tag{16}$$

The governing equation of motion Eq.(13), along with the associated interface stress expression Eq.(2) can be solved numerically. If the perfectly plastic model is used for soil reinforcement pull-out resistance, T_g, the unit resistance of the reinforced soil system becomes

$$R(u) = R_{\max} = \frac{T_g\, b}{b\, h} = \frac{T_g}{h} \tag{17}$$

When the deceleration of the panel from connection to soil reinforcement is less than the deceleration of the incident shock, the interface stress becomes tensile and the wall panel tends to pull the soil reinforcement out from the soil. The soil reinforcement must carry the tension developed at the interface. If the wall panel stays in contact with soil, the reinforced soil system is termed "compression controlled." The displacement of the wall panel was found (Tuan and Merkle 1993) to be:

$$u(t) = \frac{2\sigma_o}{\alpha \rho C_L}\left(1 + \frac{\alpha}{\eta - \alpha} e^{-\eta t} - \frac{\eta}{\eta - \alpha} e^{-\alpha t}\right) - \frac{R_{\max}}{\rho C_L \eta}\left(\eta t - 1 + e^{-\eta t}\right) \tag{18}$$

and the interface stress as

$$\sigma_i(t) = 2\sigma_o\left(\frac{\eta}{\eta - \alpha} e^{-\eta t} - \frac{\alpha}{\eta - \alpha} e^{-\alpha t}\right) + R_{\max}\left(1 - e^{-\eta t}\right) \tag{19}$$

where the parameter

International Journal of Geomechanics. Submitted January 29, 2013; accepted July 24, 2013;
posted ahead of print July 26, 2013. doi:10.1061/(ASCE)GM.1943-5622.0000342

$$\eta = \frac{\rho c_L}{\rho_w d} \tag{20}$$

If the wall panel separates from the soil, the reinforced soil system is termed "tension controlled" and Eq.(13) has to be solved numerically. A relationship between the ratio η / α and the ratio $\sigma_o / R_{\max}$ is shown in Figure 4. This relationship can be used to determine whether separation will occur.

The peak free-field soil displacement can be determined from Eq.(16) to be

$$u_{ff} = \frac{\sigma_o}{\alpha \rho c_L} \tag{21}$$

The maximum lateral wall panel translation, $u_{\max}$, for a compression controlled system is always less than twice the peak free-field soil displacement. However, a large wall panel displacement may occur for a tension controlled system. Figure 5 shows a normalized displacement envelope in terms of η / α and $\sigma_o / R_{\max}$ for both compression and tension controlled systems.

FULL-SCALE MSE WALL EXPLOSIVE TESTS

Four reinforced soil walls were constructed and subject to six explosive tests to evaluate the effects of the soil reinforcement stiffness and the standoff distance of the explosion. Detailed accounts of the walls construction, construction materials, instrumentation plan, test procedures, and data reduction are provided by Reid (1995). The full-scale wall test matrix is given in Table 1.

The Reinforced Soil Test Walls

International Journal of Geomechanics. Submitted January 29, 2013; accepted July 24, 2013;
posted ahead of print July 26, 2013. doi:10.1061/(ASCE)GM.1943-5622.0000342

The full-scale test walls were 5 m (16.8 ft) high with 55 cm (1.8 ft) embedment depth, and 24 m (79 ft) wide at the base, as shown in Figure 6. The dimensions of the various facing panels are given in Table 2. These panels were 14 cm (5.5 in.) thick and based on the 2,370 kg/m^3 (148 pcf) density, the masses of these panels are determined.

A fine sand with coefficient of uniformity C_u = 1.63 and particle size D_{50} = 0.24 mm (0.01 in.) was used for backfill. The maximum dry unit weight was 1,630 kg/m^3 (102 pcf) at 11.3% water content. The angle of the internal friction was 33 degrees. Two types of geogrids, UX1400HT and UX1500HT by Tensar Corporation were used for soil reinforcement. Two layers of geogrids were cast in each concrete facing panel, each layer rolled out for a 3.7-m (12-ft) embedment length and between 76-cm (2.5-ft) soil lifts. A total of six layers of geogrids are laid within a 5.5-m (18-ft) wide and 3.8-m (12.5-ft) high central portion of the wall (shaded area in Figure 6), which was under the maximum interface pressure from the explosion and consequently was used for validation of the analytical model.

The Blast Loading

An explosive charge of 120 kg (264 lbs) of TNT (equivalent) was placed at various standoff distances from the back of the concrete panels given in Table 1. The explosive, a 1.5-m (5-ft) long cylinder, was placed vertically in the backfill such that its center was located 2.3 m (7.5 ft) from the top of the wall. The explosive was placed in the vertical plane of symmetry of the wall. The standoff distance was adjusted in the subsequent tests based on the sensor data and wall damage from the first test.

Test Results

International Journal of Geomechanics. Submitted January 29, 2013; accepted July 24, 2013;
posted ahead of print July 26, 2013. doi:10.1061/(ASCE)GM.1943-5622.0000342

A comprehensive instrumentation plan was carried out to acquire wall panel accelerations a, soil/panel interface pressures σ_i, geogrid strains, and free-field soil pressures σ_{ff} in each test. The loading wave velocity of the soil was determined from the shock front arrival times in the data traces. The average loading wave velocity c_L from all the tests was 306 m/s (1,004 ft/s). The average peak data from the tests are given in Table 3. The strain gages on the geogrids did not yield useful information due to insufficient recording time. Almost all the geogrid strains were compressive, indicating that the geogrids were compressed along with the surrounding soil upon initial shock wave arrival. Geogrids would have taken the tensile stresses from the reflected stress wave off the concrete wall panels at a later time. The composite action of the geogrids would become active then if there was still confining soil pressure on the geogrids.

MODEL VALIDATION

Since the composite action of the geogrids was not effective initially, the resistance R_{max} can only be estimated from the concrete panels (Drake et al. 1989) to be about 1224 psf (8.5 psi). The specific impulses i were calculated from integrating the interface stress data traces. The theoretical decay rate α of the incident blast wave or the radial soil stress can be determined from the specific impulse by trial and error:

$$i = \int_0^{t_d} \sigma_i(t)\,dt = \int_0^{t_d} \sigma_o e^{-\alpha t}\,dt = \frac{\sigma_o}{\alpha}\left(1 - e^{-\alpha t_d}\right) \tag{22}$$

The derived results from these wall tests are shown in Table 4, where the symbols have been defined in the Notation. It is clear that all the tests except test No.1 are compression-controlled per Figure 4. The calculated peak panel displacements using Eq.(18) are compared against the

International Journal of Geomechanics. Submitted January 29, 2013; accepted July 24, 2013;
posted ahead of print July 26, 2013. doi:10.1061/(ASCE)GM.1943-5622.0000342

test data in Table 4. The calculated interface stress σ_i using Eq.(19) are also compared against the test data therein. It should be noted that test walls No.2 and 3 were subject to two consecutive explosive tests and the data from the latter tests were influenced by the damages from the first tests.

The explosive tests revealed the importance of standoff distances as illustrated in Figure 7. When there was a close-in explosion in the backfill, the spherical cavity expansion emanating from the explosive ejected soil above the explosive and created a crater, as shown in Figure 7(a). As a result, the geogrids became ineffective due to the loss of soil confining pressure and the upward momentum of the ejecta (i.e., the geogrids and soil) caused the wall panels to overturn.

NUMERICAL ANALYSIS

Since some data from the explosive tests were questionable, a transient dynamic analysis using the ANSYS finite element code is conducted to compare with the predictions from the analytical model. Test number 2 from the full-scale wall tests is selected as the test case. A two-dimensional finite element representation is shown in Figure 8(a). The wall panel is 152-cm (60-in.) high and 14-cm (5.5-in.) thick, connected to two layers of geogrids embedded in the soil. The length for the ground shock propagation through the reinforced soil medium is 365 cm (144 in.). The geogrids are anchored on the left end and attached to the wall panel on the right end, and the geogrids are assumed free to slide relative to the soil medium. A triangular pulse of peak pressure of 70 kPa (10 psi) with no rise time and a duration of 0.003 s (i.e., $\boldsymbol{i}$ = 0.015 psi-sec) is applied on the left soil boundary at t = 0.001 s. The unit weights of the soil and the concrete panel are 1730 kg/m^3 (108 pcf) and 2370 kg/m^3 (148 pcf), respectively.

International Journal of Geomechanics. Submitted January 29, 2013; accepted July 24, 2013;
posted ahead of print July 26, 2013. doi:10.1061/(ASCE)GM.1943-5622.0000342

The soil and concrete panel are respectively modeled with 2880 and 40 of the 8-node PLANE183 elements, and the geogrids with 72 LINK11 elements. The FE model consists of a total of 2992 elements and 9165 nodes. All the elements are assumed to be linearly elastic. The elastic stiffness of the soil, concrete panel, and the geogrids are 220 MPa (31,920 psi), 23.5 GPa (3.4×10^6 psi), and 17.5 kN/m (100 lb/in.), respectively. The elastic stiffness of the geogrids was determined from the same strain energy amount by the perfectly plastic resistance, R_{max}. Figure 8(b) presents the time-history of the theoretical normal stress at the interface between the soil and the wall panel. It is interesting to see the reverberations of shock wave between the soil boundary and the wall panel for a duration of 0.1 s, though only the first spike would exist in reality. It takes 0.012 s for the shock front to arrive at the wall panel. The peak stress is 90 kPa (13 psi) as compared to 137 kPa (19.84 psi) from the closed-form solution given in Table 4. The maximum wall panel displacement of 0.05 cm (0.02 in.) takes place when the panel velocity is zero at t = 0.03 s. The snapshot of the displacement field of the entire model at t = 0.03 s is shown in Figure 8(c). This value compares closely with 0.062 cm (0.0246 in.) given in Table 4. The accuracy of the closed-form solution is thus clearly verified by the finite element analysis. It is noted that the peak interface stresses in Tests 3 and 4 were 109 kPa (15.83 psi) and 73 kPa (10.53 psi), measured in similar ground shock environments as Test 2.

CONCLUSIONS

The use of MSE wall systems for protective structures has received attention for their energy absorbing capability and blast resistance. The free-field soil stress and ground shock motion depend upon the energy release from the explosion, standoff from the wall, mechanical properties of the reinforced soil, and depth of burial of the explosive. The analytical model

International Journal of Geomechanics. Submitted January 29, 2013; accepted July 24, 2013;
posted ahead of print July 26, 2013. doi:10.1061/(ASCE)GM.1943-5622.0000342

proposed in this study provides a simple method for predicting the dynamic interaction between reinforced soil and wall panels under ground shock loading.

The maximum resistance of a MSE wall depends mainly on its energy absorbing capacity and rate of energy dissipation. Therefore, the connection between wall panels and soil reinforcement, and soil reinforcement itself should have adequate ductility and high tensile strength. Furthermore, the soil reinforcement should also have high tensile modulus to minimize the wall panel displacement. Since differences exist between the maximum panel displacements and the interface stresses predicted by the analytical model and from the wall test data, the accuracy of the analytical model have been further validated against transient dynamic finite element analysis results. Given the complexity of the given problem, the SDOF analytical model is deemed adequate for preliminary design purposes.

International Journal of Geomechanics. Submitted January 29, 2013; accepted July 24, 2013;
posted ahead of print July 26, 2013. doi:10.1061/(ASCE)GM.1943-5622.0000342

NOTATION

The following symbols are used in this paper:

a = peak wall panel acceleration;

b = width of wall panel;

c = elastic wave propagation velocity of reinforced soil;

c_L = loading wave velovity of soil;

d = thickness of wall panel;

$F(t-T)$ = Heaviside step function;

F_v = shear and frictional forces between interlocking wall panels;

H = height of MSE wall;

h = height of wall panel;

i = specific impulse of interface stress time-history;

j = integer numbers;

K_x = constrained bulk modulus of reinforced soil;

$K(u)$ = structural stiffness of wall panel/soil reinforcement;

M = mass of wall panel;

m, p, q = intermediate variables;

R = standoff distance of the MSE wall from the explosive;

$R(u)$ = structural resistance per unit area of wall panel;

R_{max} = pull-out resistance of soil reinforcement or maximum resistance of MSE wall;

s = a complex variable in the Laplace domain;

T = time of arrival of the shock wave;

International Journal of Geomechanics. Submitted January 29, 2013; accepted July 24, 2013;
posted ahead of print July 26, 2013. doi:10.1061/(ASCE)GM.1943-5622.0000342

T_g = pull-out resistance of geogrids attached to a wall panel;

t = time;

t_d = duration of the interface stress time-history;

t_1, t_2, t_3 = time of arrival of incident and reflected stress wave fronts;

$U(x,s)$ = soil particle displacement $u(x,t)$ after Laplace transform, $0 \le x \le R$;

u_{ff} = free-field soil displacement at $x = R$ as if retaining wall was not there;

$u(t)$ = displacement of wall panel at $x = R$;

u_{max} = maximum wall panel displacement at $x = R$;

$\dot{u}(t)$ = velocity of wall panel at $x = R$;

$\ddot{u}(t)$ = acceleration of wall panel at $x = R$;

V_{ff} = free-field soil particle velocity at $x = R$ as if retaining wall was not there;

v_o = initial soil particle velocity at shock front at $x = 0$;

x = distance along the direction of wave propagation and normal to wall panels;

α = attenuation rate of ground shock;

$\beta, \gamma, \theta, \mu, \eta, \xi, \omega$ = intermediate variables;

$\Delta V(t)$ = velocity differential between free-field particle velocity and velocity of wall panel;

λ = ratio of maximum unit resistance of wall to constrained modulus of reinforced soil;

ρ = mass density of reinforced soil;

ρ_w = mass density of wall panel;

σ_{ff} = free-field soil norml stress at $x = R$ as if retaining wall was not there;

σ_o = initial soil normal stress at shock front at $x = 0$; and

International Journal of Geomechanics. Submitted January 29, 2013; accepted July 24, 2013;
posted ahead of print July 26, 2013. doi:10.1061/(ASCE)GM.1943-5622.0000342

σ_i = normal stress on the interface between the reinforced soil and wall panel at $x = R$.

International Journal of Geomechanics. Submitted January 29, 2013; accepted July 24, 2013;
posted ahead of print July 26, 2013. doi:10.1061/(ASCE)GM.1943-5622.0000342

APPENDIX – CLOSED FORM SOLUTION BY THE LAPLACE TRANSFORM METHOD

Taking the Laplace transform of Eqs.(3), (5), and (7) respectively yields

$$\frac{\partial^2 U(x,s)}{\partial x^2} - \frac{s^2}{c^2} U(x,s) = 0 \tag{A-1}$$

$$U(0,s) = \frac{v_o}{s(s+\alpha)} \tag{A-2}$$

$$\mu s^2 U(R,s) + \frac{\partial U(R,s)}{\partial x} + \frac{\lambda}{s} = 0 \tag{A-3}$$

where s is a complex variable in the Laplace domain, and x is held fixed throughout the transformation.

Using the following variables,

$$t_1 = t - \frac{x}{c} \tag{A-4}$$

$$t_2 = \left(t + \frac{x}{c}\right) - 2T \tag{A-5}$$

$$t_3 = \left(t - \frac{x}{c}\right) - 2T \tag{A-6}$$

$$T = \frac{R}{c} \tag{A-7}$$

$$m = \mu \alpha c \tag{A-8}$$

$$p = m + 1 \tag{A-9}$$

$$q = m - 1 \tag{A-10}$$

$$\gamma = \frac{1}{\mu c} \tag{A-11}$$

$$\xi = \mu c^2 \tag{A-12}$$

International Journal of Geomechanics. Submitted January 29, 2013; accepted July 24, 2013;
posted ahead of print July 26, 2013. doi:10.1061/(ASCE)GM.1943-5622.0000342

The solution of Eqs.(A-1) through (A-3) is

$$U(x,s)=\frac{v_o}{s(s+\alpha)}\left[\cosh\theta-\left(\frac{\sinh\beta+\mu sc\times\cosh\beta}{\cosh\beta+\mu sc\times\sinh\beta}\right)\sinh\theta\right]$$

$$-\left(\frac{c\lambda/s^2}{\cosh\beta+\mu sc\times\sinh\beta}\right)\sinh\theta \qquad \text{(A-13)}$$

where

$$\beta = \frac{sR}{c} \qquad \text{(A-14)}$$

and

$$\theta = \frac{sx}{c} \qquad \text{(A-15)}$$

The particle displacement, $u(x, t)$, is obtained by taking the inverse transform of Equation (A-13), rewritten in the form of

$$U(x,s)=\frac{v_o}{s(s+\alpha)}\left(e^{\theta}-\frac{e^{\theta}-e^{-\theta}}{1+\omega}\right)-\frac{c\lambda}{s^2}\left(\frac{e^{-\beta}}{1+\mu sc}\right)\left(\frac{e^{\theta}-e^{-\theta}}{1+\omega}\right) \qquad \text{(A-16)}$$

where

$$\omega = \left(\frac{1-\mu sc}{1+\mu sc}\right)e^{-2\beta} \qquad \text{(A-17)}$$

Since $\omega<1$,

$$\frac{1}{1+\omega} = \sum_{j=0}^{\infty}(-1)^j\,\omega^j \qquad \text{(A-18)}$$

and

$$U(x,s)=\frac{v_o}{s(s+\alpha)}\left[e^{\theta}-\left(e^{\theta}-e^{-\theta}\right)\sum_{j=0}^{\infty}(-1)^j\,\omega^j\right]-\frac{c\lambda}{s^2}\left(\frac{e^{-\beta}}{1+\mu sc}\right)\left[\left(e^{\theta}-e^{-\theta}\right)\sum_{j=0}^{\infty}(-1)^j\,\omega^j\right]$$

(A-19)

International Journal of Geomechanics. Submitted January 29, 2013; accepted July 24, 2013;
posted ahead of print July 26, 2013. doi:10.1061/(ASCE)GM.1943-5622.0000342

Keeping only the first three terms of the infinite series (i.e., j = 0, 1, and 2), the particle displacement can be expressed as

$$u(x,t) = \sum_{i=1}^{3} u_i \tag{A-20}$$

the u_i terms in Equation (A-20) are given as follows:

$$\begin{aligned} u_1 &= 0 && (t_1 < 0) \\ &= \frac{v_o}{\alpha}\left(1 - e^{-\alpha t_1}\right) && (t_1 > 0) \end{aligned} \tag{A-21}$$

$$\begin{aligned} u_2 &= 0 && (t_2 < 0) \\ &= -\frac{v_o}{\alpha q}\left[p\left(1 - e^{-\alpha t_2}\right) - 2m\left(1 - e^{-\gamma t_2}\right)\right] - \lambda\left[c t_2 - \xi\left(1 - e^{-\gamma t_2}\right)\right] && (t_2 > 0) \end{aligned} \tag{A-22}$$

$$\begin{aligned} u_3 &= 0 && (t_3 < 0) \\ &= \frac{v_o}{\alpha q}\left[p\left(1 - e^{-\alpha t_3}\right) - 2m\left(1 - e^{-\gamma t_3}\right)\right] + \lambda\left[c t_3 - \xi\left(1 - e^{-\gamma t_3}\right)\right] && (t_3 > 0) \end{aligned} \tag{A-23}$$

The expressions for normal stress, particle velocity, particle acceleration of the reinforced soil medium can be readily derived from Eqs.(A-21) through (A-23). Although higher order terms could be added to the solution, the transient response of the reinforced soil system due to shock loading will be damped out rapidly.

International Journal of Geomechanics. Submitted January 29, 2013; accepted July 24, 2013; posted ahead of print July 26, 2013. doi:10.1061/(ASCE)GM.1943-5622.0000342

REFERENCES

An, J., Tuan, C.Y., Cheeseman, B.A., and Gazonas, G.A. (2011). "Simulation of Soil Behavior under Blast Loading," International Journal of Geomechanics, ASCE, 11(4), July/August 2011, pp.323-334.

Berg, R.R., Christopher, B.R., and Samtani, N.C. (2009). Design and Construction of Mechanically Stabilized Earth Walls and Reinforced Soil Slopes - Volume I, FHWA-NHI-10-024, Federal Highway Administration, McLean, VA, November 2009, 306p.

Crawford, R.E., Higgins, C.J., and Bultmann, E.H. (1974). The Air Force Manual for Design and Analysis of Hardened Structures, AFWL-TR-74-102, Air Force Weapons Laboratory, Kirtland AFB, NM.

Drake, J.L., and Little, C.D. (1983). "Ground Shock from Penetrating Conventional Weapons," Proceedings of the Symposium on Interaction of Non-nuclear Munitions with Structures, U.S. Air Force Academy, Colorado, May 10-13, 1983, pp.1-6.

Drake, J.L., and Rochefort, M.A. (1987). "Response of Buried Structure Walls to Earth Penetrating Conventional Weapons," Dynamics of Structures, ASCE, August 1987, pp.455-468.

Drake, J.L., Twisdale, L.A., Frank, R.A., Dass, W.C., Rochefort, M.A., Walker, R.E., Britt, J.R., Murphy, C.E., Slawson, T.R., and Sues, R.H. (1989). "Protective Construction Design Manual," Report Number ESL-TR-87-57, Air Force Engineering and Services Center, Tyndall Air Force Base, Florida, November 1989.

Esmaeili, M., Nik, M.G., and Khayyer, F. (2012). "Experimental and Numerical Study of Micropiles to Reinforce the High Railway Embankments," Int. Journal of Geomechanics, ASCE, DOI:10.1061/(ASCE)GM.1943-5622.0000280 (Dec. 17, 2012).

International Journal of Geomechanics. Submitted January 29, 2013; accepted July 24, 2013;
posted ahead of print July 26, 2013. doi:10.1061/(ASCE)GM.1943-5622.0000342

Giang, N.H., Kuwano, J., . Izawa, J., and Tachibana, S. (2010). "Influence of unloading–reloading processes on the pullout resistance of geogrid," Geosynthetics International, Volume 17, Issue 4, August 2010.

Grujicic, M., Pandurangan, B., Cheeseman, B.A., Roy, W.N., and Skaggs, R.R. (2008). "Parameterization of the porous material model for sand with different levels of water saturation," Soil Dynamics and Earthquake Engineering, 28: 20-35.

Raudanski, E., Eytan, R., and Sweiry, G. (1990). "Reinforced Soil Ammunition Magazine, Full-scale Tests-1990, Testing Program," Headquarters, Israeli Air Force Civil Engineering Division, Engineering and Products Branch.

Reid, R.A. (1995). "Conventional Weapons Effects on Reinforced Soil Walls," A Ph.D. Dissertation, Department of Civil Engineering, Georgia Institute of Technology, Atlanta, GA, March 1995, 390p.

Richardson, G.N., Feger, D., Fong, A., and Lee, K.L. (1977). "Seismic Testing of Reinforced Earth Walls," J. of the Geotechnical Engrg. Div., ASCE, Vol. 103, No.GTI, Jan. 1977, pp.1-17.

Tuan, C.Y., and Merkle, D.H. (1993). "Advanced Panel and Connection System for Reinforced Soil," ESL-TR-92-76, Engineering Research Division, U.S. Air Force Civil Engineering Support Agency, Tyndall Air Force Base, Florida, March 1993, 106 p.

Wang, Z., and Lu, Y. (2003). "Numerical analysis on dynamic deformation mechanism of soils under blast loading," Soil Dynamics and Earthquake Engineering, 705-714.

J. Zhou, J., Chen, J.-F., Xue, J.-F., and Wang, J.-Q. (2012). "Micro-mechanism of the interaction between sand and geogrid transverse ribs," Geosynthetics International, Volume 19, Issue 6, December 2012.

International Journal of Geomechanics. Submitted January 29, 2013; accepted July 24, 2013;
posted ahead of print July 26, 2013. doi:10.1061/(ASCE)GM.1943-5622.0000342

Captions of Figures

1. **Protective Shelter constructed with Reinforced Soil**
2. **Free-body Diagram of a Panel with Two-layers of Geogrids**
3. **A Single-Degree-of-Freedom Model**
4. **Prediction of Compressive or Tensile Interface Stress**
5. **Maximum Wall Displacement to Peak Free-field Soil Displacement**
6. **Front View of the Test Reinforced Soil Wall**
7. **Close-in Standoff caused Wall Collapse**
8. **Numerical Analysis of Ground Shock Propagation between Reinforced Soil and Wall Panel**
   - **(a) Finite Element Model of Reinforced Soil Wall**
   - **(b) Interface Stress Time-history between Soil and Wall panel**
   - **(c) Snapshot of the Displacement Field at t = 0.03 s**

International Journal of Geomechanics. Submitted January 29, 2013; accepted July 24, 2013;
posted ahead of print July 26, 2013. doi:10.1061/(ASCE)GM.1943-5622.0000342

Figure 1. Protective Shelter constructed with Reinforced Soil

International Journal of Geomechanics. Submitted January 29, 2013; accepted July 24, 2013;
posted ahead of print July 26, 2013. doi:10.1061/(ASCE)GM.1943-5622.0000342

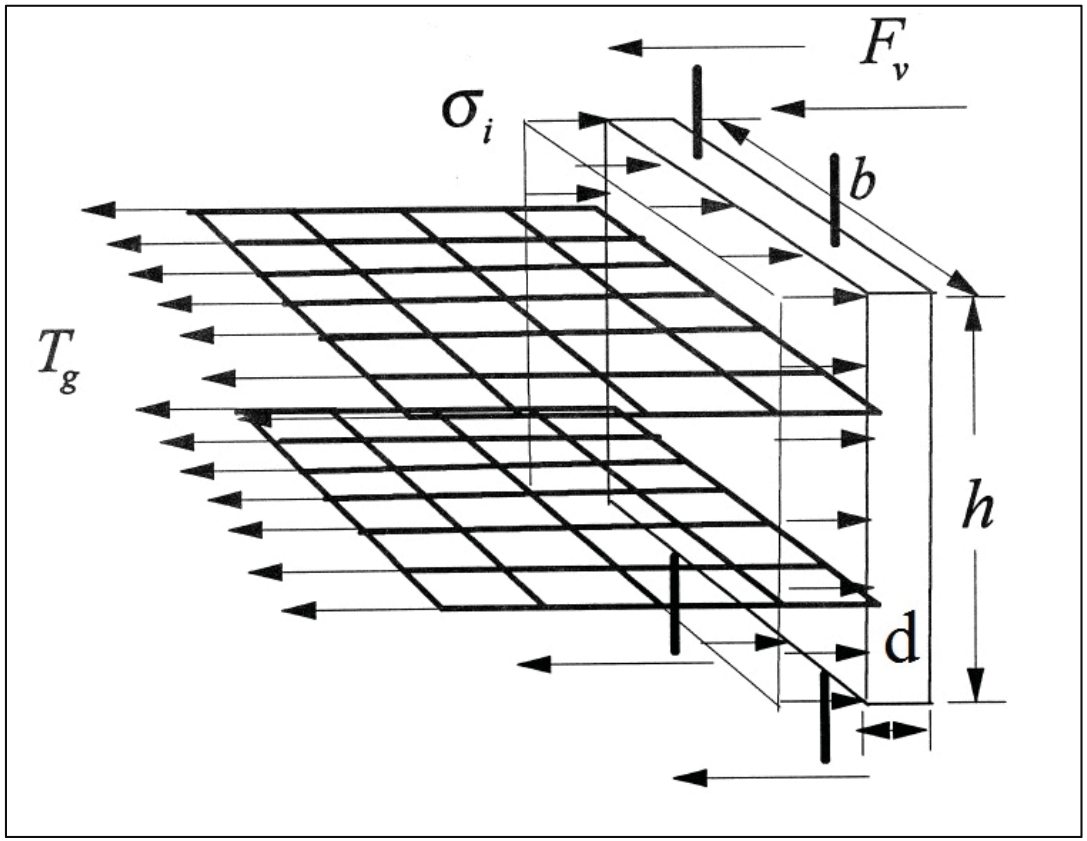

Figure 2. Free-body Diagram of a Panel with Two-layers of Geogrids

International Journal of Geomechanics. Submitted January 29, 2013; accepted July 24, 2013;
posted ahead of print July 26, 2013. doi:10.1061/(ASCE)GM.1943-5622.0000342

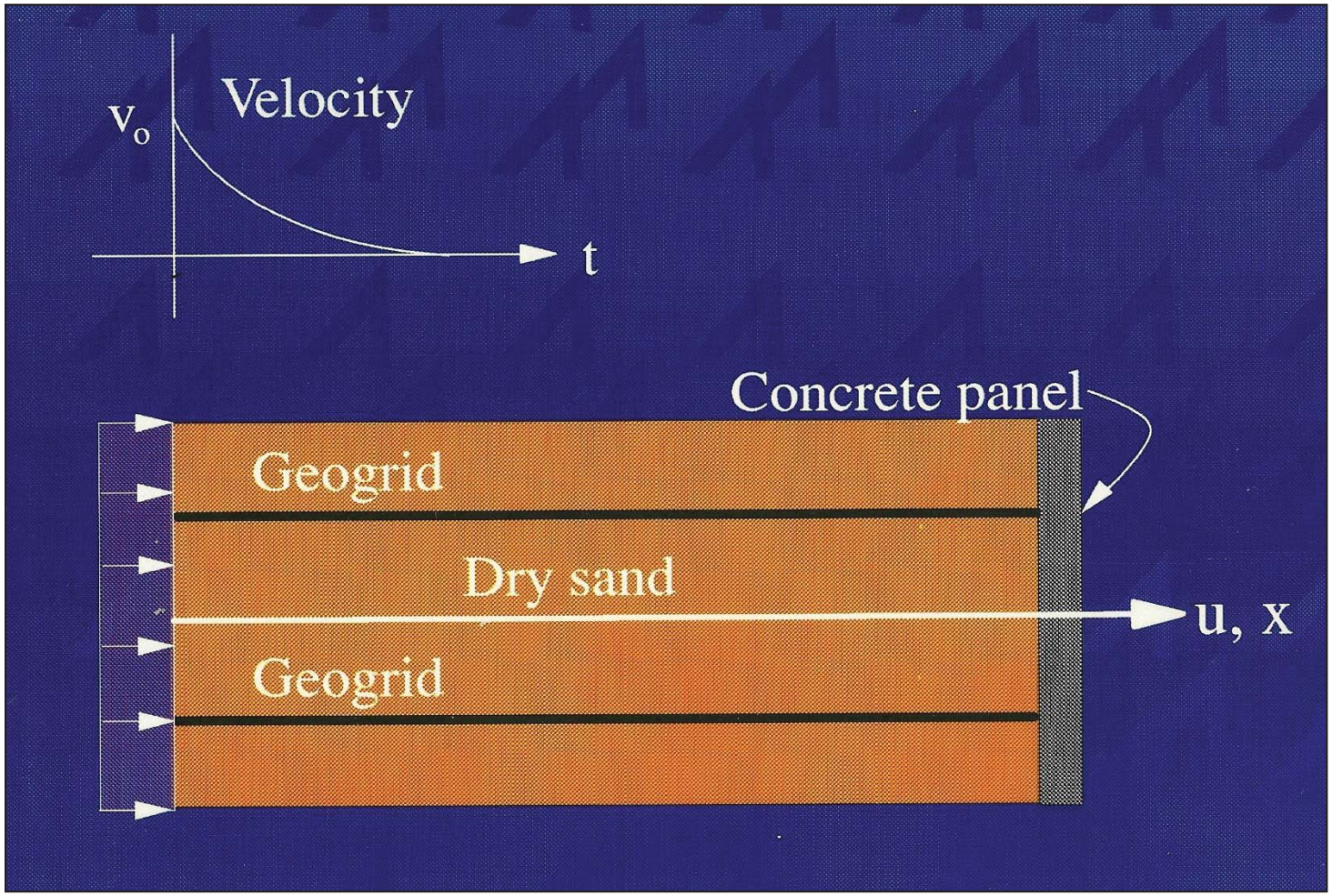

Figure 3. A Single-Degree-of-Freedom Model

International Journal of Geomechanics. Submitted January 29, 2013; accepted July 24, 2013;
posted ahead of print July 26, 2013. doi:10.1061/(ASCE)GM.1943-5622.0000342

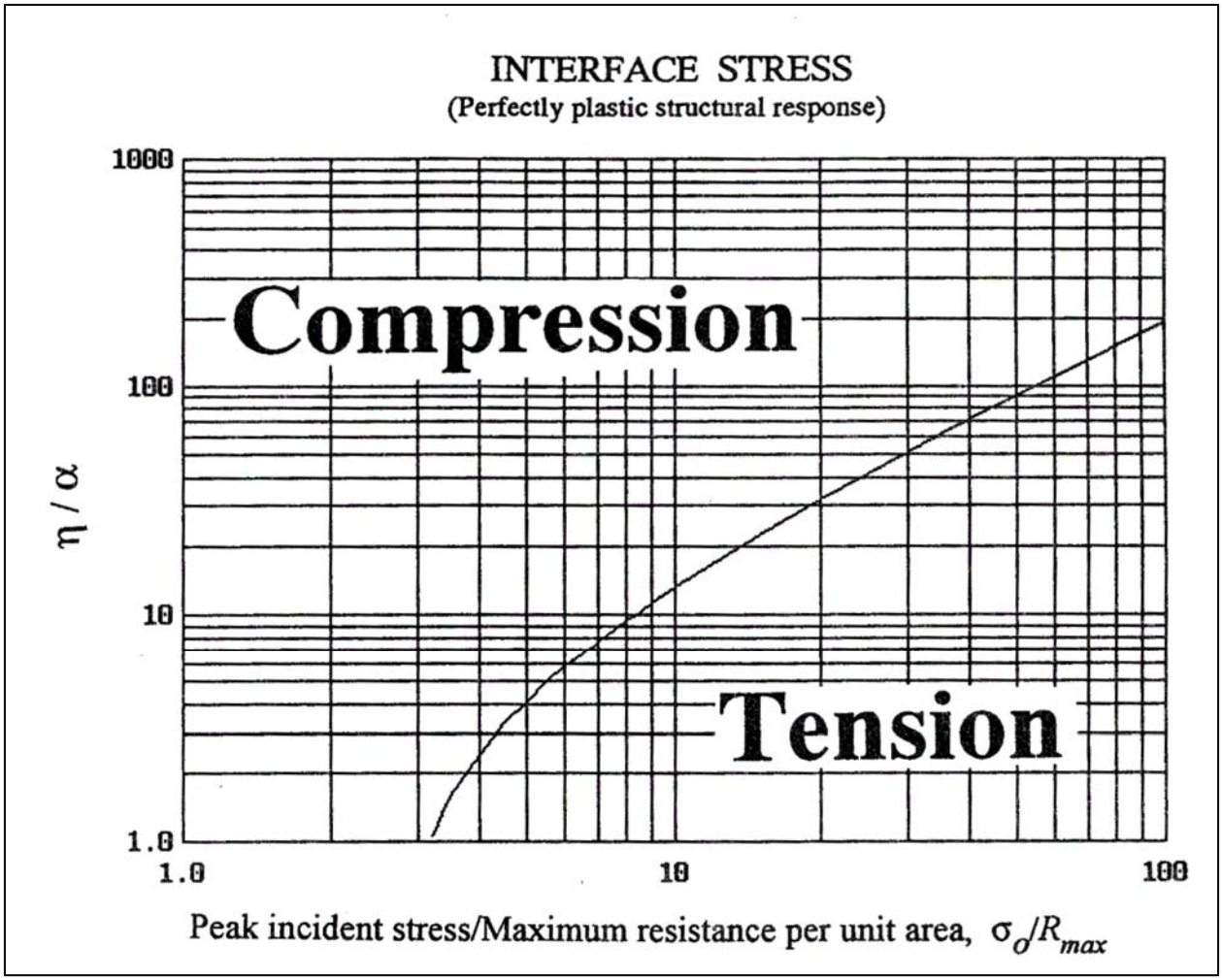

Figure 4. Prediction of Compressive or Tensile Interface Stress

International Journal of Geomechanics. Submitted January 29, 2013; accepted July 24, 2013;
posted ahead of print July 26, 2013. doi:10.1061/(ASCE)GM.1943-5622.0000342

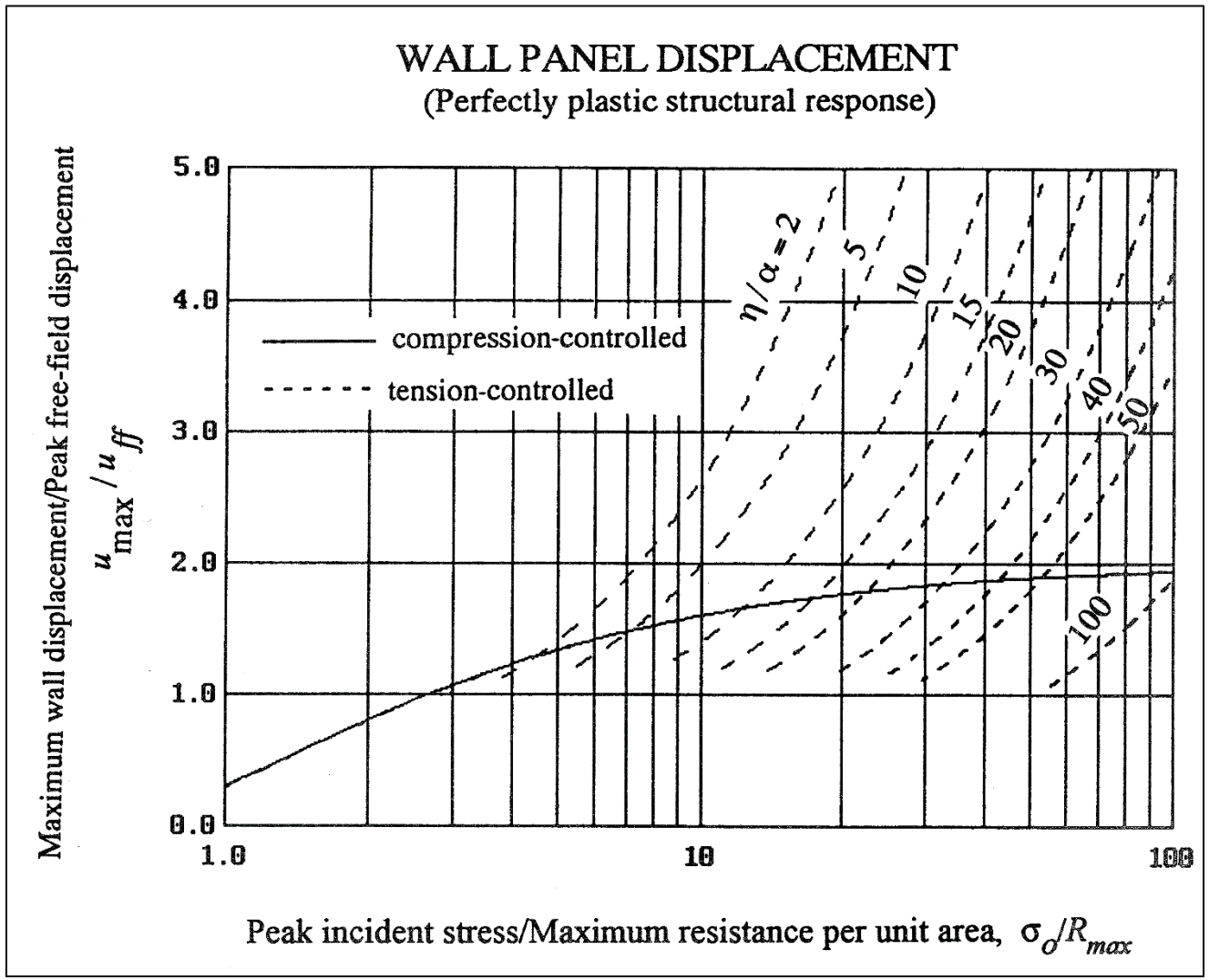

Figure 5. Maximum Wall Displacement to Peak Free-field Soil Displacement

Figure 6

International Journal of Geomechanics. Submitted January 29, 2013; accepted July 24, 2013;
posted ahead of print July 26, 2013. doi:10.1061/(ASCE)GM.1943-5622.0000342

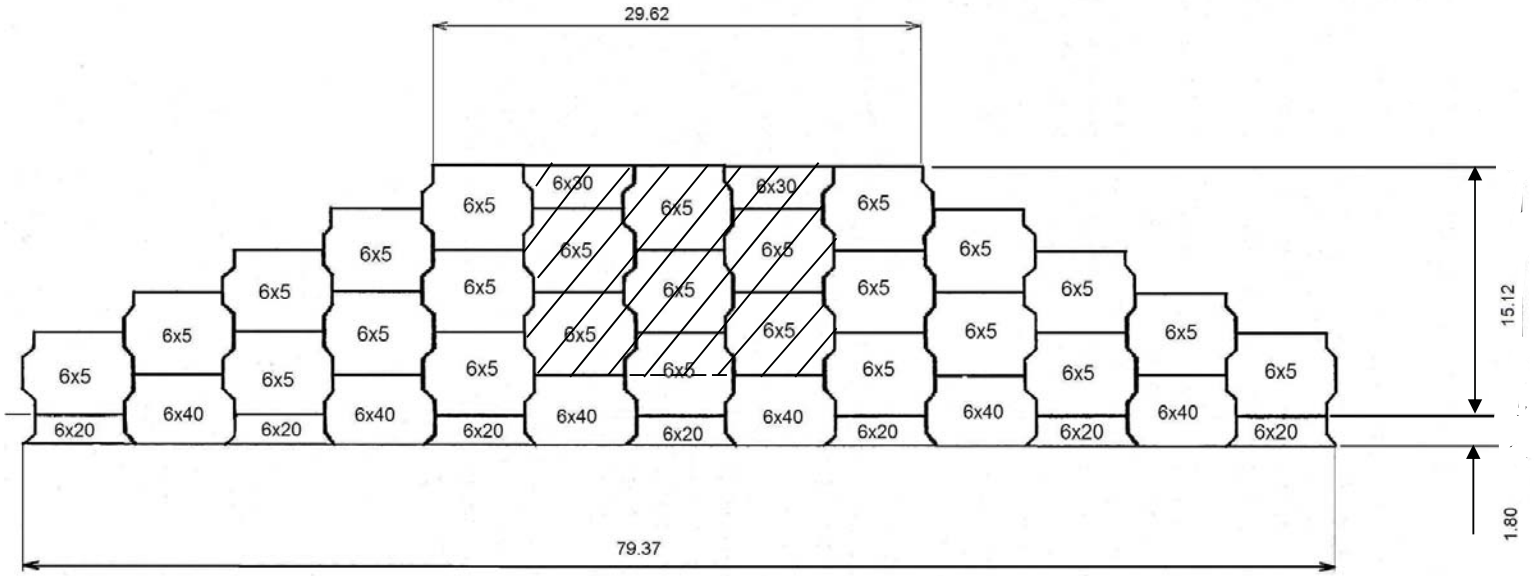

Dimensions in Feet (1 ft = 0.3 m)

Figure 6. Front View of the Test Reinforced Soil Wall

International Journal of Geomechanics. Submitted January 29, 2013; accepted July 24, 2013;
posted ahead of print July 26, 2013. doi:10.1061/(ASCE)GM.1943-5622.0000342

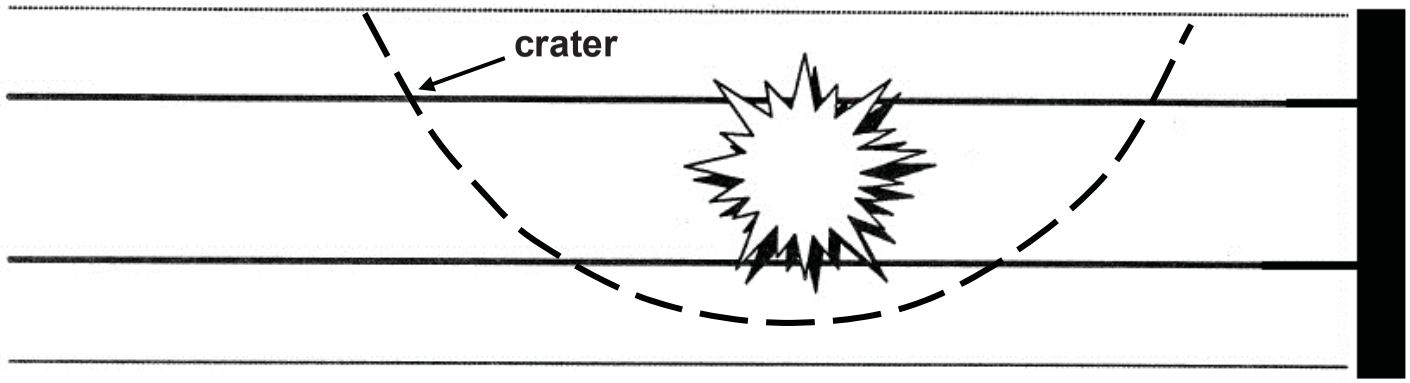

(a) Explosion within Reinforced Soil

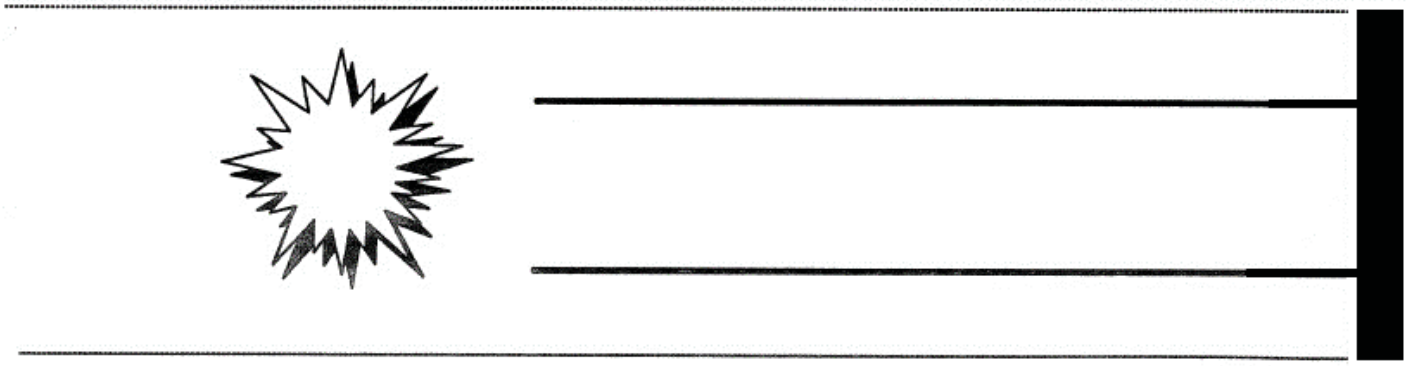

(b) Explosion beyond Reinforced Soil

Figure 7. Close-in Standoff caused Wall Collapse

Figure 8

International Journal of Geomechanics. Submitted January 29, 2013; accepted July 24, 2013;
posted ahead of print July 26, 2013. doi:10.1061/(ASCE)GM.1943-5622.0000342

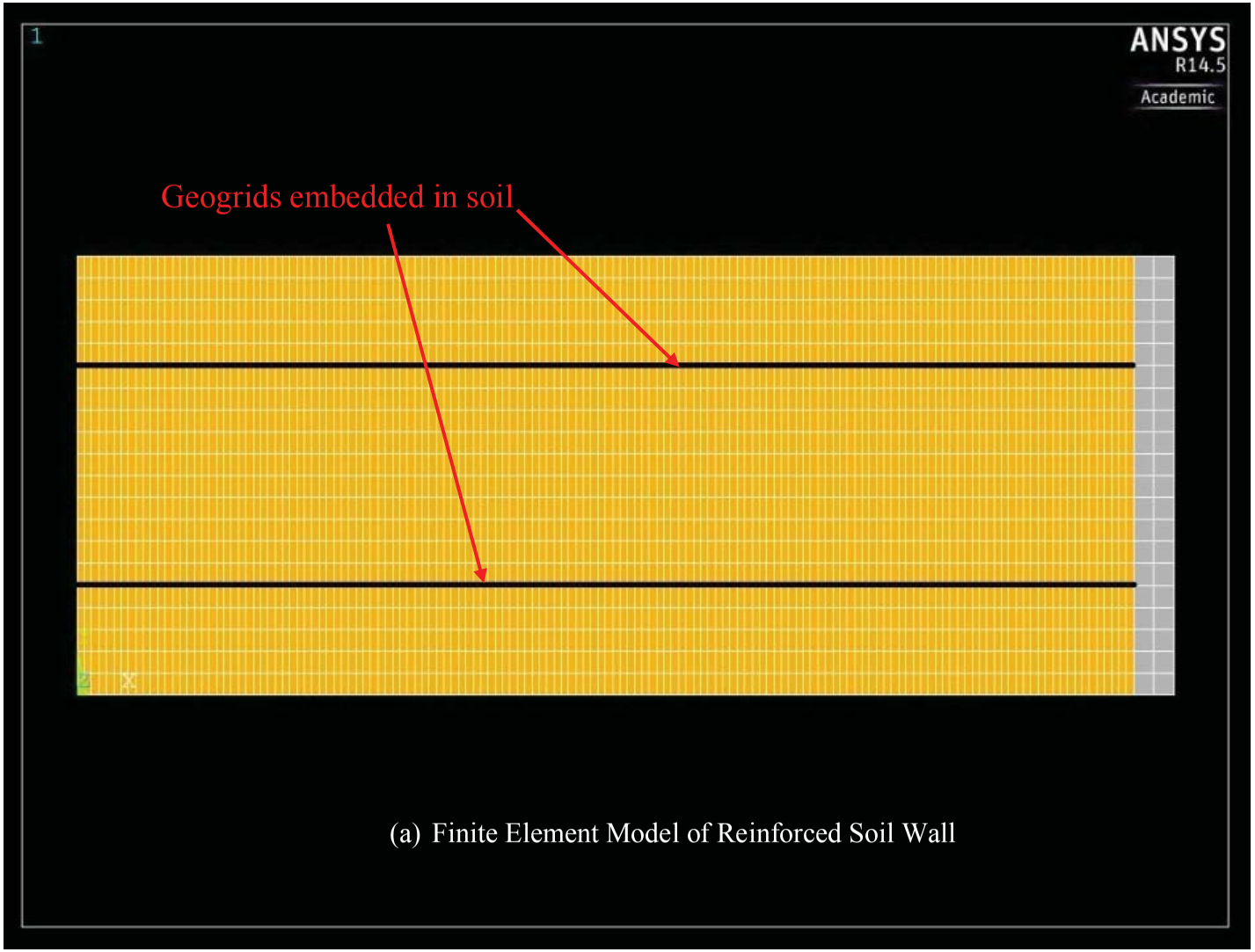

(a) Finite Element Model of Reinforced Soil Wall

International Journal of Geomechanics. Submitted January 29, 2013; accepted July 24, 2013;
posted ahead of print July 26, 2013. doi:10.1061/(ASCE)GM.1943-5622.0000342

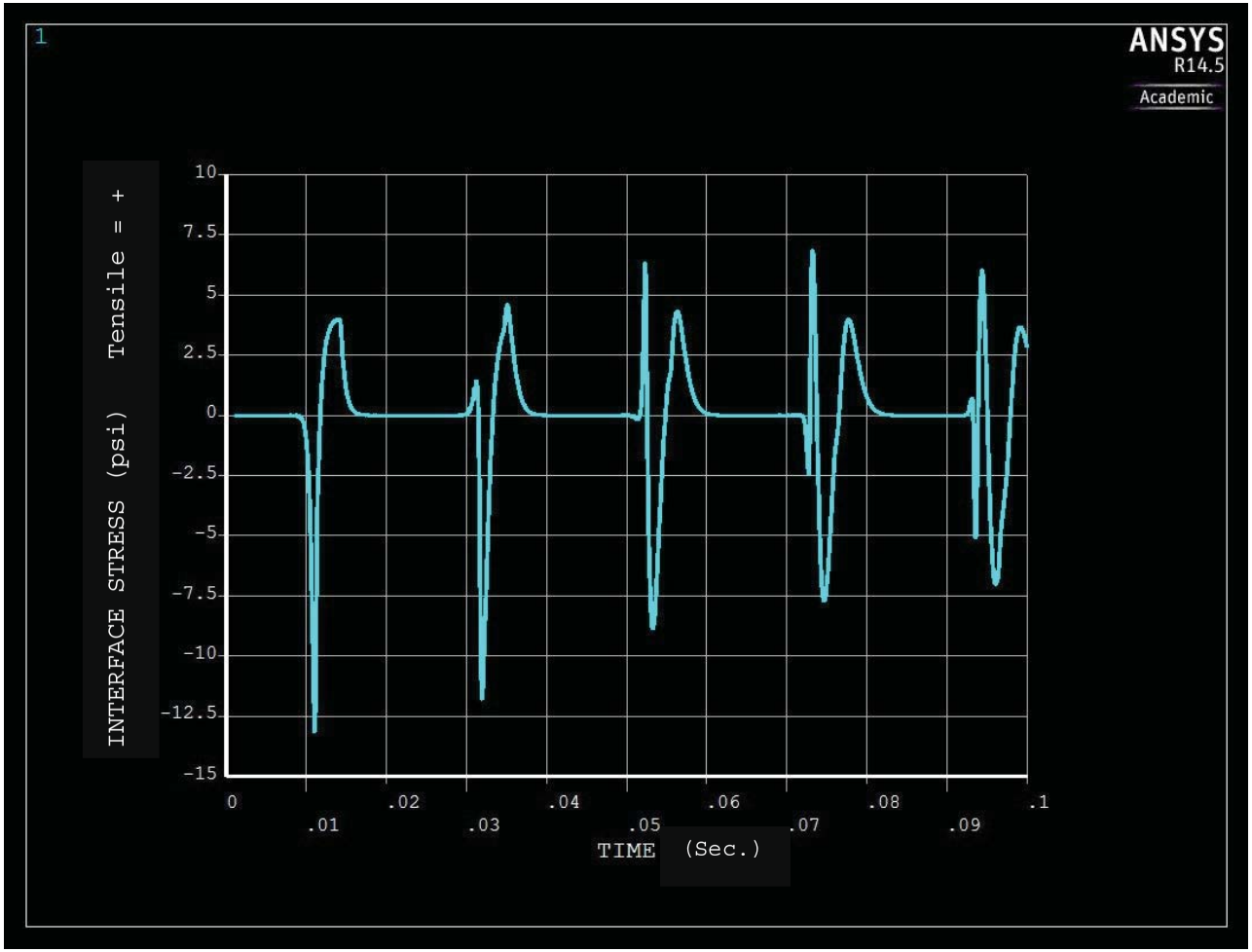

(b) Interface normal stress between soil and wall panel

International Journal of Geomechanics. Submitted January 29, 2013; accepted July 24, 2013;
posted ahead of print July 26, 2013. doi:10.1061/(ASCE)GM.1943-5622.0000342

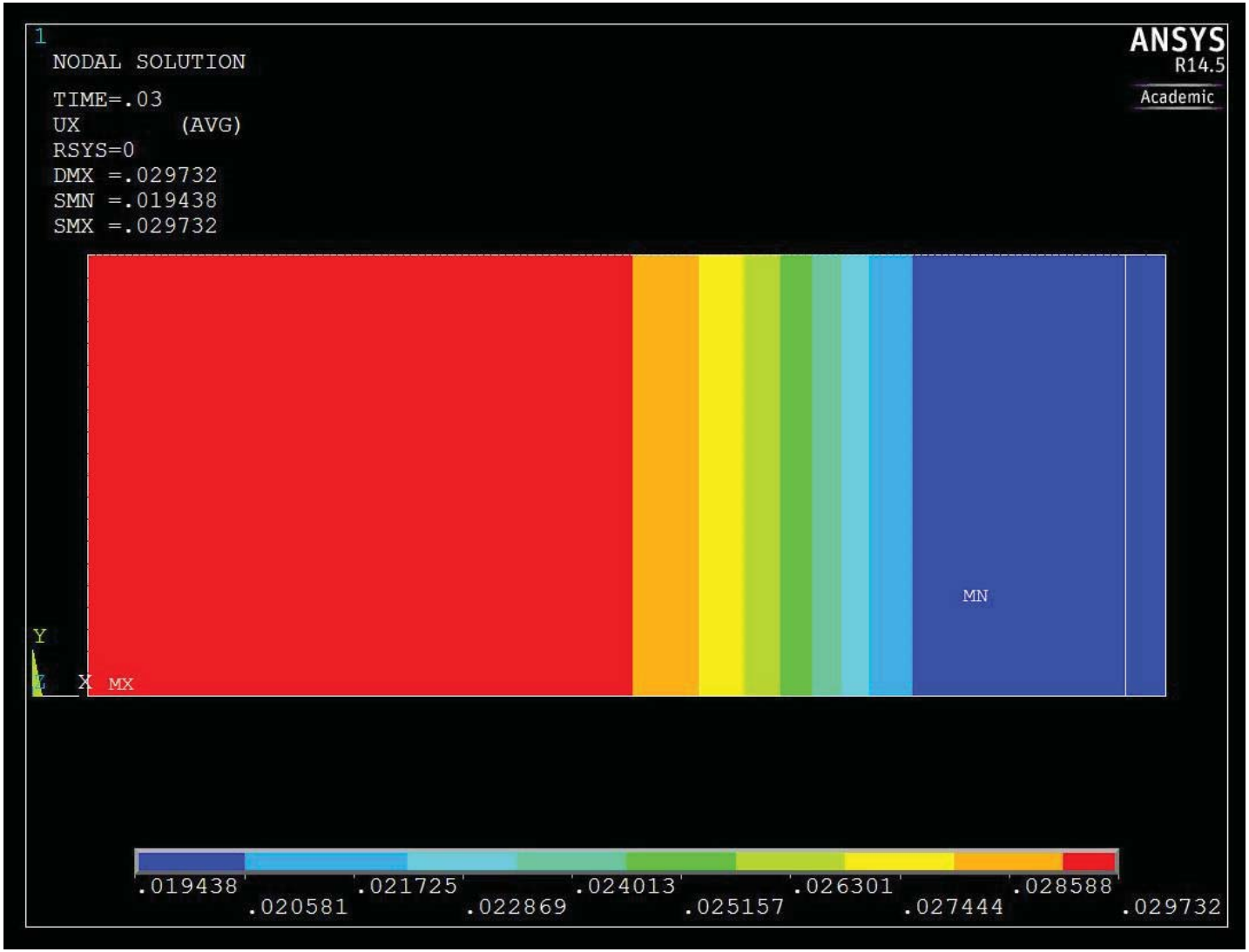

(c) Snapshot of Displacement Field at time = 0.03 s

Figure 8. Numerical Analysis of Ground Shock Propagation between Reinforced Soil and Wall Panel

International Journal of Geomechanics. Submitted January 29, 2013; accepted July 24, 2013;
posted ahead of print July 26, 2013. doi:10.1061/(ASCE)GM.1943-5622.0000342

Table 1. Full-scale Wall Test Matrix (Reid 1995)

Test No.	Wall No.	Geogrid	Standoff (ft)	Result
1	1	UX1400HT	20	Wall failed
2	2	UX1400HT	30	Wall survived
3	2	UX1400HT	25	Wall failed
4	3	UX1500HT	30	Wall survived
5	3	UX1500HT	25	Wall survived
6	4	UX1500HT	20	One panel failed

Note: 1 ft = 0.3 m

International Journal of Geomechanics. Submitted January 29, 2013; accepted July 24, 2013;
posted ahead of print July 26, 2013. doi:10.1061/(ASCE)GM.1943-5622.0000342

Table 2. Dimensions and Masses of Panel Shapes

	Dimensions (cm)			
Panel Shape	**Height**	**Width**	**Thickness**	**Mass (kg)**
6×5	152	202	14	925
6×40	127	202	14	770
6×30	75	202	14	465
6×20	46	202	14	280

Note: Panel shapes are shown in Figure 7.

International Journal of Geomechanics. Submitted January 29, 2013; accepted July 24, 2013;
posted ahead of print July 26, 2013. doi:10.1061/(ASCE)GM.1943-5622.0000342

Table 3. Full-scale Wall Test Data (Reid 1995)

Test Number	σ_o (psi)	i (psi-sec)	α (sec^{-1})	σ_i (psi)	ρ (pcf)	c_L (ft/s)	a (g's)
1	62.2	0.0316	152.3	11.06	108.8	1066	31.1
2	9.92	0.0148	86.2	3.80	108.0	1000	14.5
3	9.18	0.0595	114.2	15.83	108.0	935	14.8
4	10.54	0.0503	92.5	10.53	105.7	1085	10.8
5	16.98	0.0660	161.7	11.50	105.7	936	21.2

(1) No data was available in Test No.6 due to data logger malfunction.
(2) The mass density of facing panels, ρ_w = 148 pcf.

International Journal of Geomechanics. Submitted January 29, 2013; accepted July 24, 2013;
posted ahead of print July 26, 2013. doi:10.1061/(ASCE)GM.1943-5622.0000342

Table 4. Maximum Wall Panel Displacements

Test Number	η (sec^{-1})	η / α	σ_o / R_{max}	u_{ff} (in.)	u_{max} / u_{ff}	$u_{max}^{\S}$ (in.)	u_{max}^{*} (in.)	$\sigma_i^{\S}$ (psi)	σ_i^{*} (psi)
1	1706	11.20	7.32	0.1959	1.39	0.2731	0.0066	12.40	11.06
2	1589	18.43	1.17	0.0593	0.41	0.0246	0.0047	19.84	3.80
3	1486	13.01	1.08	0.0443	0.36	0.0158	0.0046	18.36	15.83
4	1687	18.24	1.24	0.0553	0.46	0.0254	0.0057	21.08	10.53
5	1455	9.00	2.00	0.0591	0.80	0.0474	0.0170	33.96	11.50

§ Peak values from Eqs.(18) and (19).

* Peak values from wall tests (Reid 1995).